Near-Field Beam Focusing for Wireless Power Transfer With Dynamic Metasurface Antennas

Haiyang Zhang, *Member, IEEE*, Nir Shlezinger, *Senior Member, IEEE*, Francesco Guidi, *Member, IEEE*, Anna Guerra, *Member, IEEE*, Davide Dardari, *Fellow, IEEE*, Mohammadreza F. Imani, *Member, IEEE*, and Yonina C. Eldar, *Fellow, IEEE*

***Abstract*—Radio frequency wireless power transfer enables charging low-power mobile devices without relying on wired infrastructures. Current existing wireless power transfer systems are typically designed assuming far-field propagation, where the radiated energy is steered to towards given angles, resulting in limited efficiency and possible radiation in undesired locations. An emerging technology for wireless signaling is based on dynamic metasurface antennas (DMAs), which efficiently realize electrically large arrays. When such arrays are employed at high frequencies, wireless power transfer might take place in the radiating near-field (Fresnel) region, where spherical wave propagation holds, providing more degrees-of-freedom and improved performance. In this article, we study wireless power transfer systems charging multiple devices in the Fresnel region, where the energy transmitter is equipped with a DMA, exploring how the antenna configuration can exploit the spherical wavefront to generate focused energy beams. In particular, after presenting a mathematical model for DMA-based radiating near-field wireless power transfer systems, we characterize the weighted sum-harvested energy maximization problem of the considered system, and we propose an efficient solution to jointly design the DMA weights and digital precoding vector. Then, by accounting for hardware constraints, we further extend our study to encompass practical scenarios with discrete phase shifts in DMA elements. Simulation results show that our design generates focused energy beams capable of improving energy transfer efficiency in the radiating near-field with minimal energy pollution.**

***Index Terms*—Beam focusing, dynamic metasurface antennas (DMAs), radiating near-field, wireless power transfer.**

Received 29 December 2024; revised 10 March 2025; accepted 21 March 2025. Date of publication 26 March 2025; date of current version 9 June 2025. The work of Haiyang Zhang was supported in part by the open research fund of National Mobile Communications Research Laboratory, Southeast University under Grant 2025D09; and in part by Natural Science Research Start-up Foundation of Recruiting Talents of Nanjing University of Posts and Telecommunications under Grant NY223031. The work of Nir Shlezinger was supported by the European Research Council (ERC) under the ERC starting Grant 101163973 (FLAIR). The work of Davide Dardari was supported by the HORIZON-JU-SNS-2022 project TIMES under Grant 101096307. The work of Francesco Guidi and Davide Dardari were supported in part by the European Union under the Italian National Recovery and Resilience Plan (NRRP) of NextGenerationEU, partnership on "Telecommunications of the Future" under Grant PE00000001—program "RESTART". The work of Anna Guerra was supported by the European Union under the ERC starting under Grant 101116257 (CUE-GO). The work of Yonina C. Eldar was supported by the European Union's H2020 Research and Innovation Program under Grant 646804-ERC-COG-BNYQ. This article was presented in part at the IEEE 23rd International Workshop on Signal Processing Advances in Wireless Communication (SPAWC), Oulu, Finland, July 2022 [DOI: 10.1109/SPAWC51304.2022.9833917]. *(Corresponding author: Haiyang Zhang.)*

Haiyang Zhang is with the School of Communication and Information Engineering, Nanjing University of Posts and Telecommunications, Nanjing 210049, China, and also with the National Mobile Communications Research Laboratory, Southeast University, Nanjing 210096, China (e-mail: haiyang.zhang@njupt.edu.cn).

Nir Shlezinger is with the School of ECE, Ben-Gurion University, Be'er Sheva 84105, Israel (e-mail: nirshl@bgu.ac.il).

Francesco Guidi is with the National Research Council of Italy, IEIIT, 40136 Bologna, Italy (e-mail: francesco.guidi@cnr.it).

Anna Guerra and Davide Dardari are with DEI-Wilab-CNIT, University of Bologna, 40126 Bologna, Italy (e-mail: anna.guerra3@unibo.it; davide.dardari@unibo.it).

Mohammadreza F. Imani is with the School of ECEE, Arizona State University, Tempe, AZ 85287 USA (e-mail: mohammadreza.imani@asu.edu).

Yonina C. Eldar is with the Faculty of Math and CS, Weizmann Institute of Science, Rehovot 76100, Israel (e-mail: yonina.eldar@weizmann.ac.il).

Digital Object Identifier 10.1109/JIOT.2025.3555113

I. Introduction

INTERNET of Everything (IoE) is one of the major applications of future 6G wireless communication networks [1], [2]. The fact that many IoE devices connected to the network are either battery-powered or battery-less [3] gives rise to the need to energize them in a simple and efficient manner. Radio frequency (RF) wireless power transfer is regarded as a promising technology for charging IoE devices, by utilizing RF signals to wirelessly and simultaneously power multiple devices. Compared with the near-field reactive-based wireless power transfer techniques, such as inductive coupling and magnetic resonance coupling, which require the charged device to be very close to the energy source, RF-based wireless power transfer is capable of charging devices in a more flexible way over longer distances. Hence, RF-based wireless power transfer presents many potential applications for supporting and prolonging the operation of IoE devices in in-home setups, as well as in industrial and commercial settings, where a large number of distributed sensors require maintenance-free power [4].

To date, RF wireless power transfer is mainly studied for charging devices residing in the far field region [5]. In such cases, given the antennas' size, the operational distance between the energizing transmitter and the receivers is larger than the Fraunhofer distance, and thus the radiating wavefront obeys the conventional plane wave model. Far-field transmitters can only direct energy toward a given angle via beamsteering techniques, resulting in low efficiency and notable energy pollution, i.e., energy radiated at undesired locations. Nonetheless, future wireless 6G systems are expected to support an ecosystem with IoE devices at millimeter wave (mmWave) bands [6] using extremely large-scale antenna arrays [7]. The combination of large antennas and high-frequency signaling results in devices located in

distances ranging from a few centimeters to several tens of meters residing in the *radiating near-field* region [8], [9], [10].

Unlike the far-field case, where the electromagnetic (EM) field is a plane wave, in the radiating near-field region, the EM field is a spherical wavefront. Radiating near-field transmitters can generate focused beams [11], [12], which were shown to mitigate interference in multiuser communications [13] and enhance degrees-of-freedom [14]. Moreover, it was recently envisioned that this capability can facilitate efficient wireless power transfer with minimal energy pollution [15]. Subsequently, several works have studied the near-field wireless power transfer, such as [16], [17], and [18]. In particular, Mayer et al. [16] investigated the optimal placement of antennas in a MISO wireless power transfer system designed for a 3-D cuboid room within the Fresnel region. The primary focus is maximizing the received power at the worst receiver location by considering the spherical nature of the electromagnetic wavefronts in the Fresnel region. Demarchou et al. [17] considered a near-field channel model to achieve power beam focusing at a predefined focal point, while Deutschmann et al. [18] studied reciprocity-based beamforming to enhance the power transfer efficiency with large-scale multiple-input-multiple-output (MIMO). Moreover, motivated by the far-field concept of simultaneous wireless information and power transfer (SWIPT), several works have also explored using the near-field beamfocusing capability to enhance both communication and wireless power transfer efficiency [19], [20], [21], [22].

The aforementioned works primarily focus on near-field wireless power transfer enabled by fully digital antenna architectures. While fully digital architectures, where each antenna element is connected to a dedicated RF chain, are considered the most flexible antenna arrays, implementing fully digital large-scale antennas is increasingly challenging due to high power consumption and implementation costs [23]. A widely studied alternative is the hybrid analog/digital architecture, which combines low-dimensional digital signal processing with high-dimensional analog precoding [24], [25]. By using fewer RF chains than antenna elements, hybrid architectures achieve reductions in cost and power consumption compared to fully digital solutions [26]. However, these architectures typically rely on phase shifters and other active analog components, which can still limit scalability and hinder the realization of extremely large-scale antenna arrays.

A promising emerging technology for implementing large-scale arrays is dynamic metasurface antennas (DMAs) [27], [28]. DMAs leverage the unique properties of metamaterials to dynamically control electromagnetic wave propagation [29]. Compared to traditional architectures, DMAs offer several advantages. Specifically, they provide programmable control of transmit and receive beam patterns while inherently reducing the number of required RF chains, without the need for dedicated analog circuitry [30]. This capability not only lowers hardware complexity and energy consumption, but makes DMAs an attractive and efficient option for realizing extremely large-scale antenna arrays, while often being simpler to implement compared to hybrid MIMO and providing additional forms of analog signal processing [31], [32], [33], [34]. Specifically, Shlezinger et al. [35] analyzed the fundamental limits of uplink communications using DMAs, and demonstrated that the achievable rate with DMAs is comparable to that of ideal fully digital antenna arrays. This motivates the exploration of the potential to achieve energy focusing using the emerging antenna architecture of DMAs.

In this work, we study radiating near-field wireless power transfer when the energy transmitter uses an extremely large-scale DMA, quantifying its capability to charge multiple remote devices with minimal energy pollution by forming focused energy beams. To the best of our knowledge, this work is the first study on near-field beam focusing for multiuser wireless power transfer with DMAs, facilitating simultaneous power charging of multiple energy receivers. The main contributions of this article can be summarized as follows.

1) We first formulate a mathematical model for DMA-based near-field multiuser wireless power transfer systems that incorporates the DMAs processing and the propagation of the transmitted EM waves in near-field wireless channels. Based on this model, we aim to optimize the digital precoding vector and the DMA weights for maximizing the weighted sum-harvested energy when working in the radiating near-field region, while accounting for the specific Lorentzian-form response of metamaterial elements.
2) To design the radiating near-field transmission pattern based on the weighted sum-harvested energy maximization objective, we propose an alternating optimization algorithm to deal with the corresponding nonconvex optimization problem. In particular, we provide a closed-form optimal digital precoding solution for a fixed DMA configuration. Then, we recast the DMA elements design problem into a Riemannian manifold optimization problem, which we efficiently solve using the Riemannian conjugate gradient (RCG) approach.
3) In real-world implementations, the phase shifts of DMA elements are inherently discrete due to the physical limitations of the metamaterials. To address this aspect, we further extend our study by incorporating discrete phase shifts into the DMA beamfocusing design. Specifically, this analysis bridges the gap between idealized theoretical models and practical hardware implementations, offering a more realistic study of DMA-enabled near-field wireless power transfer systems.
4) Simulation results verify that our proposed design effectively focus transmissions to the desired focal points, demonstrating its energy-focusing capability under both ideal continuous and practical discrete phase shift scenarios. Furthermore, we show that by leveraging the beamfocusing capabilities of DMAs, the proposed approach can intelligently and efficiently charge multiple users based on their priority or requirements while minimizing energy pollution and waste.

The remainder of this article is organized as follows. Section II models DMA-based radiating near-field wireless power transfer systems and formulates the sum-harvested power maximization problem. Section III presents an efficient

algorithm for tuning the DMA weights. Section IV accounts for discrete phase shifts in DMA elements to fit more practical scenarios. Section V provides numerical results to demonstrate the performance of the proposed design under both continuous and discrete phase scenarios. Finally, Section VI concludes the article.

We use boldface lower case and upper case letters for vectors and matrices, respectively. The ℓ_2 norm, vectorization, transpose, conjugate, and Hermitian transpose, are denoted as $\|\cdot\|$, $\text{vec}(\cdot)$, $(\cdot)^{\text{T}}$, $(\cdot)^{\dagger}$, and $(\cdot)^{H}$, respectively, and $\mathbb{C}$ is the set of complex numbers.

II. System Model

In this section, we characterize the mathematical model for DMA-based radiating near-field wireless power transfer. We begin by introducing the DMA transmission model in Section II-A. Then, we present the near-field wireless channel model in Section II-B, and formulate the harvested power maximization problem in Section II-C.

A. Dynamic Metasurface Antennas

DMA is an emerging technology for realizing large-scale antenna arrays using reconfigurable metamaterials, whose physical properties, such as permittivity and permeability are dynamically adjustable [30]. These antenna architectures are typically comprised of multiple microstrips, each containing multiple metamaterial elements. The frequency response of each element is independently adjustable by varying its local dielectric properties [28]. For DMA-based transmitters, each microstrip is fed by an RF chain, and the input signal is radiated to all the elements within the same microstrip [36].

To model the transmission procedure, consider a DMA with N_d microstrips of N_e elements each, i.e., the total number of tunable metamaterial elements is $N \triangleq N_d \cdot N_e$. Letting $\mathbf{z}_f \in \mathbb{C}^{N_d \times 1}$ denote the input signals to the microstrips, the radiated signal, denoted by $\mathbf{r}$, can be written as

$$\mathbf{r} = \mathbf{H}\mathbf{Q}\,\mathbf{z}_f. \tag{1}$$

Here, $\mathbf{Q} \in \mathbb{C}^{N \times N_d}$ is the configurable DMAs weights, whose entries are

$$\mathbf{Q}_{(i-1)N_e+l,n} = \begin{cases} q_{i,l}, & i = n \\ 0, & i \neq n \end{cases} \tag{2}$$

where $q_{i,l}$ denotes the frequency response of the lth metamaterial element of ith microstrip. These responses satisfy the Lorentzian form [37], approximated as

$$q_{i,l} \in \mathcal{Q} \triangleq \left\{ \frac{j + e^{j\phi}}{2} \,|\, \phi \in [0, 2\pi] \right\} \qquad \forall i, l. \tag{3}$$

In addition, $\mathbf{H}$ in (1) is a $N \times N$ diagonal matrix with entries $\mathbf{H}_{((i-1)N_e+l,(i-1)N_e+l)} = h_{i,l}$, where $h_{i,l}$ denotes the signal propagation effect of the lth metamaterial element of ith microstrip (inside the microstrip). These coefficients can be written as $h_{i,l} = e^{-\rho_{i,l}(\alpha_c + j\beta_c)}$, where α_c and β_c are two constants depending on the characteristic of DMA, and $\rho_{i,l}$ denotes the location of the lth element in the ith microstrip.

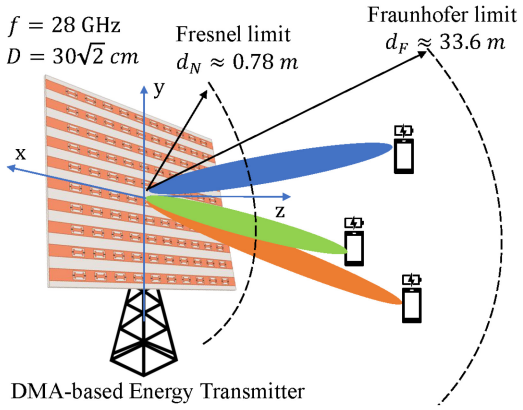

Fig. 1. Illustration of the proposed DMA-based near-field wireless power transfer system, where multiple energy receivers are located within the near-field region of DMA.

B. DMA-Based Near-Field Channel Model

We consider a radiating near-field multiuser MIMO wireless power transfer system where a DMA-based energy transmitter wirelessly charges M single-antenna energy receivers, as illustrated in Fig. 1. For the radiating near-field case, the distance between the DMA transmitter and the energy receivers is assumed to be not larger than the Fraunhofer distance $d_F \triangleq [2D^2/\lambda]$ and not smaller than the Fresnel limit $d_N \triangleq \sqrt[3]{[D^4/8\lambda]}$ [8], with D and λ representing the antenna diameter and the wavelength, respectively. The properties of spherical waves in the radiating near-field allow for the generation of focused beams that facilitate wireless power transfer [11].

To formulate the overall energy transmission model, we let e_m be the unit-power energy symbol for the mth energy receiver, $m \in \{1, 2, \ldots, M\} \triangleq \mathcal{M}$, and use $\mathbf{w}_m \in \mathbb{C}^{N_d \times 1}$ to denote the digital precoding vector. The digital input to the DMA is given by $\mathbf{z}_f = \sum_{m=1}^{M} \mathbf{w}_m e_m$, and thus, from (1), the radiated signal can be expressed as

$$\mathbf{r} = \sum_{m=1}^{M} \mathbf{H}\mathbf{Q}\,\mathbf{w}_m e_m. \tag{4}$$

Let $\mathbf{p}_{i,l} = (x_i, y_l, 0)$, $i = 1, 2, \ldots N_d$, $l = 1, 2, \ldots, N_e$, denote the Cartesian coordinate of the lth element of the ith microstrip. Then, under the free-space condition, the signal received by the mth energy receiver located in $\mathbf{p}_m = (x_m, y_m, z_m)$ can be written as

$$s(\mathbf{p}_m) = \sum_{i=1}^{N_d} \sum_{l=1}^{N_e} A_{i,l}(\mathbf{p}_m)\, e^{-\jmath k d_{i,l,m}}\, y_{i,l} + n_m. \tag{5}$$

Here, $y_{i,l}$ denotes the signal emitted by the antenna at position $p_{i,l}$, $d_{i,l,m} = |\mathbf{p}_m - \mathbf{p}_{i,l}|$ is the distance between the lth element of the ith microstrip and the mth energy receiver, $k \triangleq 2\pi/\lambda$ denotes the wave number, $n_m \sim \mathcal{CN}(0, \sigma^2)$ is white Gaussian noise and $A_{i,l}(\mathbf{p}_m)$ is the path-loss coefficient. Following [38], we have $A_{i,l}(\mathbf{p}_m) = \sqrt{F(\Theta_{i,l,m})}(\lambda/4\pi d_{i,l,m})$, where $\Theta_{i,l,m} = (\theta_{i,l,m}, \phi_{i,l,m})$ is the elevation-azimuth pair from the lth element

of the ith microstrip to the mth energy receiver, and $F(\Theta_{i,l,m})$ is the radiation profile modeled as

$$F\left(\Theta_{i,l,m}\right) = \begin{cases} 2\,(b+1)\,\cos^{b}\left(\theta_{i,l,m}\right), & \theta_{i,l,m} \in \left[0, \pi/2\right] \\ 0, & \text{otherwise.} \end{cases} \quad (6)$$

In (6), the parameter b is the boresight gain constant, e.g., $b = 2$ for the dipole case [38].

For ease of analysis, we rewrite (5) in the following compact form:

$$s(\mathbf{p}_m) = \mathbf{a}_m^H \mathbf{r} + n_m$$

with

$$\mathbf{a}_m \triangleq \left[A_{1,1}(\mathbf{p}_m)\, e^{-\jmath k d_{1,1,m}}, \ldots, A_{N_d,N_l}(\mathbf{p}_m)\, e^{-\jmath k d_{N_d,N_l,m}}\right]^H.$$

Then, by using the expression for the channel input $\mathbf{r}$ given in (4), the received signal of the mth energy receiver is given by

$$s(\mathbf{p}_m) = \mathbf{a}_m^H \sum_{m=1}^{M} \mathbf{H}\mathbf{Q}\,\mathbf{w}_m e_m + n_m \quad \forall m \in \mathcal{M}. \quad (7)$$

C. Problem Formulation

Using the channel formulation (7) and the energy harvesting model proposed in [39], the harvested power from the transmitted signal of the mth energy receiver s given by

$$E_m = \zeta \sum_{j=1}^{M} \left|\mathbf{a}_m^H \mathbf{H}\mathbf{Q}\,\mathbf{w}_j\right|^2, \quad m \in \mathcal{M} \quad (8)$$

where $0 < \zeta < 1$ is the energy conversion efficiency.

Our aim is to design a transmission scheme, including both the digital precoding as well as the DMA configuration, to enable multiuser wireless power transfer in the radiating near-filed region. This is expressed as the joint optimization of the DMA weights $\mathbf{Q}$ and the digital precoding vectors $\{\mathbf{w}_m\}$ to maximize the weighted sum-harvested energy, subject to both the total transmit power constraint $P_{\max}$, and the structure constraint on the DMA weights matrix $\mathbf{Q}$ in (2), as well as the EM power leakage constraint. Mathematically, the problem of interest can be formulated as

$$\max_{\{\mathbf{w}_j\},\mathbf{Q}} \ \zeta \sum_{m=1}^{M} \alpha_m E_m$$
$$\text{s.t.} \quad (2), \quad q_{i,l} \in \mathcal{Q}\ \forall i, l, \quad \sum_{j=1}^{M} \left\|\mathbf{H}\mathbf{Q}\,\mathbf{w}_j\right\|^2 \le P_{\max} \quad (9)$$

where $\{\alpha_m\}_{m=1}^{M}$, are predefined weights that are application-specific.

III. DMA Beam Focusing for WPT

In this section, we study the joint design of the digital precoding vector and the DMA weights for maximizing the weighted sum-harvested energy. Note that (9) is nonconvex due to the coupled optimization variables in both the objective function and constraints, as well as the Lorentzian constraints on metamaterial elements. To make (9) more tractable, we relax it as follows:

$$\max_{\{\mathbf{w}_j\},\mathbf{Q}} \ \zeta \sum_{m=1}^{M}\sum_{j=1}^{M} \alpha_m \left|\mathbf{a}_m^H \mathbf{H}\mathbf{Q}\,\mathbf{w}_j\right|^2$$
$$\text{s.t.} \quad (2), \quad q_{i,l} \in \mathcal{Q}\ \forall i, l, \quad \sum_{j=1}^{M} \left\|\mathbf{w}_j\right\|^2 \le P_{\max}. \quad (10)$$

The problem (10) differs from (9) in its power constraint, which is imposed on the digital output rather than on the transmitted signal. However, one can derive the digital precoder based on (10), and scale $\{\mathbf{w}_j\}$ such that the transmitted power constraint in (9) holds.

Since problem (10) is still nonconvex, we propose to individually optimize $\mathbf{Q}$ and $\{\mathbf{w}_j\}$ in an alternating manner. In the following subsections, we show how to solve (10) for fixed $\mathbf{Q}$ and for fixed $\{\mathbf{w}_j\}$, respectively.

A. Optimizing the Digital Precoder

When $\mathbf{Q}$ is fixed, (10) reduces to the weighted sum-harvested energy maximization problem in multiuser wireless power transfer systems. By defining

$$\mathbf{G}(\mathbf{Q}) = \zeta \sum_{m=1}^{M} \alpha_m \mathbf{Q}^H \mathbf{H}^H \mathbf{a}_m \mathbf{a}_m^H \mathbf{H}\mathbf{Q}$$

the weighted sum-harvested energy can be reformulated as $\sum_{j=1}^{M} \mathbf{w}_j^H \mathbf{G}(\mathbf{Q})\,\mathbf{w}_j$. Similarly, by defining

$$\mathbf{b}_t(\mathbf{Q}) = \mathbf{Q}^H \mathbf{H}^H \mathbf{b}_t \mathbf{b}_t^H \mathbf{H}\mathbf{Q}$$

the leakaged EM power is $\sum_{j=1}^{M} \mathbf{w}_j^H \mathbf{b}_t(\mathbf{Q})\,\mathbf{w}_j$. As a result, for a fixed $\mathbf{Q}$, (10) is transformed into

$$\max_{\{\mathbf{w}_j\}} \ \sum_{j=1}^{M} \mathbf{w}_j^H \mathbf{G}(\mathbf{Q})\,\mathbf{w}_j$$
$$\text{s.t.} \quad \sum_{j=1}^{M} \left\|\mathbf{w}_j\right\|^2 \le P_{\max}. \quad (11)$$

Following [39], we have the following proposition, which provides the closed-form optimal solution to (11).

Proposition 1: Let $\mathbf{w}^*(\mathbf{Q})$ be the eigenvector corresponding to the maximal eigenvalue of $\mathbf{G}(\mathbf{Q})$. Then, (11) is maximized by setting $\mathbf{w}_j = \sqrt{p_j}\mathbf{w}^*(\mathbf{Q})$ for any nonnegative $\{p_j\}$ s.t. $\sum_{j=1}^{M} p_j = P_{\max}$.

Proposition 1 indicates that all digital precoding vectors share the same transmission direction as $\mathbf{w}^*(\mathbf{Q})$, and the total transmit power should be used to maximize the weighted sum-harvested energy. Without loss of generality, we henceforth set the digital precoder for a given $\boldsymbol{Q}$ to be

$$\mathbf{w}_1 = \sqrt{P_{\max}}\mathbf{w}^*(\mathbf{Q}), \ \text{and}\ \mathbf{w}_2 = \cdots = \mathbf{w}_M = 0. \quad (12)$$

From (12) we see that a single digital precoding vector is sufficient to maximize the weighted sum-harvested energy for a given $\boldsymbol{Q}$. This is because energy symbols do not carry information, thus each receiver can harvest energy from the same symbol.

B. Optimizing the DMA Weights

We next focus on solving (10) for fixed $\{\mathbf{w}_j\}$. According to (12), problem (10) for fixed $\{\mathbf{w}_j\}$ is simplified as

$$\max_{\mathbf{Q}} \ \zeta \ \sum_{m=1}^{M} \alpha_m \left|\mathbf{a}_m^H \mathbf{H}\mathbf{Q}\,\mathbf{w}_1\right|^2 \quad \text{s.t.} \ \ (2),\, q_{i,l} \in \mathcal{Q} \ \forall i, l. \tag{13}$$

To proceed, we define the $N_d^2 \cdot N_e \times 1$ vectors $\mathbf{q} = \text{vec}(\mathbf{Q})$, and $\mathbf{z}_m = (\mathbf{w}_1^{\mathrm{T}} \otimes (\mathbf{a}_m^H \mathbf{H}))^H$. Using these definitions, we identify an equivalent optimization problem to problem (13), as stated in following theorem.

Theorem 1: For fixed $\mathbf{w}_1$, (13) is equivalent to

$$\min_{\bar{\boldsymbol{q}}} \ \bar{\boldsymbol{q}}^H \mathbf{A}(\mathbf{w}_1)\,\bar{\boldsymbol{q}}, \quad s.t. \ \ \bar{q}_l \in \mathcal{Q} \ \forall l \in \mathcal{A}_q \tag{14}$$

where $\mathcal{A}_q$ is the set of all nonzero elements of $\mathbf{q}$, $\bar{\boldsymbol{q}}$ is the modified version of $\mathbf{q}$ obtained by removing all the zero elements of $\mathbf{q}$; $\mathbf{A}(\mathbf{w}_1) \triangleq -\zeta \sum_{m=1}^{M} \alpha_m \bar{\mathbf{z}}_m \bar{\mathbf{z}}_m^H$, with $\bar{\mathbf{z}}_m$ being the modified version of $\mathbf{z}_m$ obtained by removing the elements having the same index as the zero elements of $\mathbf{q}$.

Proof: See the Appendix. ∎

The equivalence between (13) and (14) holds in the sense that they achieve the same optimal value. Thus, the solution to (13) can be recovered from that of (14) according to the structure of $\mathbf{Q}$ (2).

Problem (14) is still nonconvex and includes the Lorentzian constraint $\bar{q}_l \in \mathcal{Q}$ defined in (3). This constraint characterizes the feasible set as a circle on the complex plane $|\bar{q}_l - (1/2)e^{j(\pi/2)}| = (1/2)$, with the circle center at $(0, [1/2]e^{j[\pi/2]})$ and radius equal to $[1/2]$. In order to simplify (14), we define a new vector variable $\mathbf{b} \in \mathbb{C}^N$ whose lth entry is given by

$$b_l = 2\bar{q}_l - e^{j\frac{\pi}{2}} \ \forall l \in \mathcal{A}_q. \tag{15}$$

The variable b_l lies on the unit circle of the complex plane, i.e., $|b_l| = 1$. According to (15), we have $\bar{\boldsymbol{q}} = [1/2](\mathbf{b} + e^{j[\pi/2]}\mathbf{1})$, where $\mathbf{1}$ denotes a $N \times 1$ all ones vector. Hence, we transform (14) into

$$\min_{\mathbf{b}} \ f(\mathbf{b}) \triangleq \frac{1}{4}\left(\mathbf{b} + e^{j\frac{\pi}{2}}\mathbf{1}\right)^H \mathbf{A}(\mathbf{w}_1)\left(\mathbf{b} + e^{j\frac{\pi}{2}}\mathbf{1}\right) \quad \text{s.t.} \ |b_l| = 1 \ \forall l \in \mathcal{A}_q. \tag{16}$$

The search space in (16) is the product of N complex circles, which is a Riemannian submanifold of $\mathbb{C}^N$. Thus, (16) can be tackled using the RCG algorithm [13], [40]. The RCG algorithm involves the following key three steps: 1) Tangent space and Riemannian gradient; 2) Vector transport; and 3) Retraction. For more details about these steps, please refer to [40] and [13].

Denote by $\mathbf{Q}$ and $\mathbf{w}_1$ as the optimal solution to problem (10). Then, we can scale $\mathbf{w}_1$ to $\mathbf{w}_1 = \sqrt{P_{\max}}(\mathbf{w}_1/\|\mathbf{H}\,\mathbf{Q}\mathbf{w}_1\|)$ such that the resulting new $\mathbf{w}_1$ and $\mathbf{Q}$ jointly represent an effective approximate solution to problem (9), satisfying the transmitted signal power constraint.

Our proposed alternating approach for solving problem (9) is summarized as Algorithm 1. In particular, in the 4th step, the updating of $\mathbf{b}^{(t+1)}$ through RCG algorithm envolves both $\mathbf{b}^{(t)}$ in step 3 as its initial value, and the Euclidean gradient of the objective $f(\mathbf{b})$ at point $\mathbf{b}$, that is

$$\nabla f(\mathbf{b}) = \frac{1}{2}\left(\mathbf{A}(\mathbf{w}_1)\,\mathbf{b} + e^{j\frac{\pi}{2}}\,\mathbf{A}(\mathbf{w}_1)\,\mathbf{1}\right)$$

for the calculation of the Riemannian gradient.

Algorithm 1 Proposed Algorithm for Solving Problem (9)

Initialize: $\mathbf{Q}^{(0)}$;
1: **for** $t = 0, 1, \ldots, T$ **do**
2: Calculate $\mathbf{w}_1^{(t)}$ based on (12), and then update $\mathbf{A}\left(\mathbf{w}_1^{(t)}\right)$;
3: Calculate $\mathbf{b}^{(t)}$ based on $\mathbf{Q}^{(t)}$ and (15);
4: Update $\mathbf{b}^{(t+1)}$ by solving problem (16);
5: Obtain $\mathbf{q}^*$ for problem (14) based on $\mathbf{b}^{(t+1)}$ and (15);
6: Update $\mathbf{Q}^{(t+1)}$ for problem (13) based on $\mathbf{q}^*$ and (2);
7: $t = t + 1$;
8: **end for**
9: $\mathbf{w}_1^* = \sqrt{P_{\max}}\,\dfrac{\mathbf{w}_1^{(T)}}{\left\|\mathbf{H}\mathbf{Q}^{(T)}\mathbf{w}_1^{(T)}\right\|}$;
Output: $\mathbf{w}_1^*$, $\mathbf{Q}^* = \mathbf{Q}^{(T)}$.

The computational complexity of Algorithm 1 can be analyzed by examining its key components. Computing the optimal digital precoder through eigenvalue decomposition requires $\mathcal{O}(N_d^3)$. Calculating the matrix $\mathbf{A}(w_1)$ involves matrix multiplications with complexity $\mathcal{O}(M \cdot N^2)$. The RCG method for optimizing the DMA weights requires $\mathcal{O}(T_1 \cdot N^2)$, where T_1 is the number of iterations needed for the RCG algorithm to converge. Therefore, with T total iterations of the alternating optimization procedure, the overall computational complexity of Algorithm 1 is $\mathcal{O}(T \cdot (N_d^3 + M \cdot N^2 + T_1 \cdot N^2))$.

IV. Extension to the Discrete DMA Configuration

In the previous sections, we investigate the DMA beam focusing design under the assumption of continuous phase shifts for the DMA elements. However, practical implementations of DMAs often necessitate the use of discrete phase shifts due to hardware constraints [41], [42], [43]. These constraints arise from the physical limitations of the metamaterials used in DMAs and the discrete nature of their control mechanisms. Therefore, in this section, we extend our study to encompass the practical scenario of discrete phase shifts in DMA elements, bridging the gap between theoretical models and real implementations.

A. Discrete DMA Model and Problem Formulation

We consider a quantized DMA model where each configurable DMA weight is encoded to realize 2^z possible phase shifts, with z denoting the number of quantization bits. The frequency response of each element (i, l) at the lth metamaterial element of the ith microstrip, denoted as $\bar{q}_{i,l}$, is constrained to a discrete set defined by [43]

$$\bar{q}_{i,l} \in \bar{\mathcal{Q}} \triangleq \left\{\frac{j + e^{j\theta}}{2} \middle| \theta = \frac{m\pi}{2^z - 1}, m \in \{0, 1, \ldots, 2^z - 1\}\right\} \forall i, l. \tag{17}$$

Note that we use $\bar{q}_{i,l}$ and $\bar{\mathcal{Q}}$ to distinguish the discrete case from the continuous case, where $q_{i,l}$ and $\mathcal{Q}$ were previously employed in (3).

Given this discrete phase shift model, we reformulate our optimization problem in (10) as follows:

$$\max_{\{\mathbf{w}_j\},\bar{\mathbf{Q}}} \ \zeta \ \sum_{m=1}^{M}\sum_{j=1}^{M}\alpha_m\left|\mathbf{a}_m^H\mathbf{H}\bar{\mathbf{Q}}\,\mathbf{w}_j\right|^2$$
$$\text{s.t.} \quad (2), \quad \bar{q}_{i,l}\in\bar{\mathcal{Q}}\ \forall i,l, \quad \sum_{j=1}^{M}\left\|\mathbf{w}_j\right\|^2\le P_{\max}. \quad (18)$$

Note that the optimization problem presented in (18) can be classified as a mixed-integer nonlinear programming problem, which is more challenging to solve compared to its continuous counterpart in (10).

B. Projection-Based Discrete DMA Configuration

In this section, we propose a projection-based approach to solve the mixed-integer nonlinear programming problem presented in (18). The key idea of the proposed method leverages the solution of the continuous DMA configuration problem and then maps it to the discrete space of DMA, followed by a refinement of the digital beamforming.

We begin by solving the problem (10) [continuous relaxation version of the problem (18)] using Algorithm 1. This step provides us with the optimal continuous DMA configuration $\mathbf{Q}^*$. Then, we project each nonzero element of $\mathbf{Q}^*$ onto the nearest discrete phase shift of DMA. This step ensures that our solution satisfies the constraint of the DMA. Specifically, for each nonzero element $q_{i,l}^*$ in $\mathbf{Q}^*$, we find the nearest discrete phase $\bar{q}_{i,l}^*$ by

$$\bar{q}_{i,l}^* = \arg\min_{\bar{q}_{i,l}\in\bar{\mathcal{Q}}}|q_{i,l}^*-\bar{q}_{i,l}|. \quad (19)$$

This projection can be efficiently implemented by comparing the phase of the complex exponential part of $q_{i,l}^*$ to the phases in $\bar{\mathcal{Q}}$ and selecting the closest match. Given that $q_{i,l}^*$ has the structure $(j+e^{j\phi}/2)$, the solution to (19) can be expressed as

$$\bar{q}_{i,l}^* = \frac{j+e^{j\frac{m^*\pi}{2^b-1}}}{2} \quad (20)$$

where $m^* = \arg\min_{m\in\{0,1,\ldots,2^b-1\}}|\phi-(m\pi/2^b-1)|$, with $\phi=\angle(2q_{i,l}^*-j)$ denoting the phase of the complex exponential part of $q_{i,l}^*$.

After obtaining the discretized DMA configuration $\bar{\mathbf{Q}}^*$, comprising elements $\{\bar{q}_{i,l}^*\}$, we update the digital beamforming weights to account for the discretization. Specifically, we update the digital precoder by solving

$$\bar{\boldsymbol{w}}_1^* = \arg\max_{\mathbf{w}} \ \sum_{m=1}^{M}\alpha_m\left|\mathbf{a}_m^H\mathbf{H}\bar{\mathbf{Q}}^*\,\mathbf{w}\right|^2$$
$$\text{s.t.} \quad \|\mathbf{w}\|^2\le P_{\max}. \quad (21)$$

This problem has a closed-form solution similar to that given in Proposition 1.

The complete algorithm for discrete DMA weight optimization can be summarized as Algorithm 2. Note that this projection-based approach leverages the efficient solution obtained for the continuous DMA case. While this method does not guarantee global optimality for the discrete problem, it consistently yields high-quality solutions in practice, as demonstrated in the subsequent numerical results section.

Algorithm 2 Projection-Based Discrete DMA Configuration

1: Obtain $\mathbf{Q}^*$ and $\mathbf{w}_1^*$ using Algorithm 1;
2: Project $\mathbf{Q}^*$ onto the discrete DMA model to obtain $\bar{\mathbf{Q}}^*$;
3: Update the digital precoder to obtain $\bar{\boldsymbol{w}}_1^*$;
Output: $\bar{\mathbf{Q}}^*$, $\bar{\boldsymbol{w}}_1^*$.

C. Discussion

The considered weighted sum-harvested energy is also a commonly used metric in conventional far-field multiuser wireless power transfer scenarios [5]. While we do not explicitly enforce the DMA to generate focused energy beams, this indeed happens when seeking to maximize the weighted sum-harvested energy, as numerically illustrated in Section V. This is because we here consider the radiating near-field scenario, where the energy beam focusing capability inherently exists, and is implicitly encapsulated in the objective via $\{\mathbf{a}_m\}$. As shown in Section V, such energy focusing brings several advantages to radiating near-field wireless power transfer systems. First, it enhances energy transfer efficiency compared with directive radiation in the far-field. Second, it reduces energy pollution and limits human exposure to radiated energy. Therefore, this capability is expected to notably facilitate the charging of 6G IoE devices in indoor settings.

For multiuser wireless communications operating in radiating near-field region with DMAs, beam focusing has been exploited to mitigate co-channel interference and hence maximize the sum-rate in our previous work [13]. Despite the similarity between multiuser near-field wireless power transfer (considered here) and communications (considered in [13]), there are several fundamental differences in both the design objectives and proposed algorithms. Specifically, for wireless communications, focused beams are designed to reduce co-channel interference which is harmful to data transmission rate. In wireless power transfer, co-channel interference is a useful energy source for energy receivers, resulting in different focused beams design considerations to fit different objectives. The fact that beam focusing designs differ between wireless power transfer and wireless communications motivates exploring SWIPT, which is a paradigm allowing a hybrid information and energy transmitter to communicate and power multiple devices at the same time [39], in the radiating near-field. However, we leave near-field SWIPT with DMAs for future work.

In addition to near-field SWIPT with DMAs, another promising research direction is the application of artificial intelligence (AI) techniques to optimize DMA configurations. The nonconvex nature of DMA optimization problems renders traditional algorithms computationally intensive, especially for extremely large-scale DMAs. AI approaches could potentially learn efficient mappings between channel information and optimal DMA configurations, thereby reducing computational

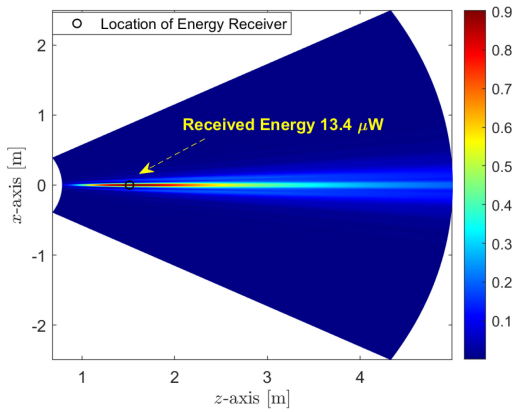

(a)

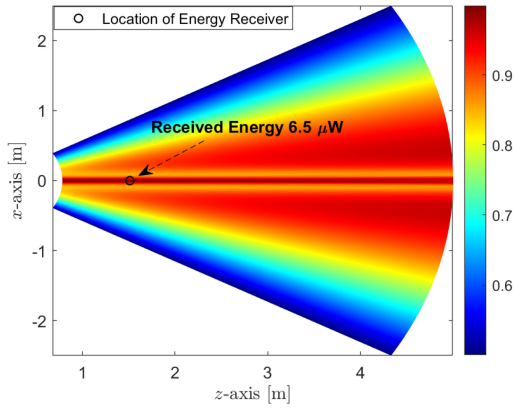

(b)

Fig. 2. Normalized received power of the energy receiver located at the: (a) near-field region and (b) far-field region.

complexity and enabling rapid adaptation to time-varying environments.

V. Numerical Evaluations

In this section, we present some representative numerical results to demonstrate the potential of energy beam focusing for radiating near-field wireless power transfer. We consider a radiating near-field wireless power transfer (WPT) system where the energy transmitter is equipped with a planar DMA positioned in the xy-plane, and the single-antenna energy receivers are positioned in the xz-plane. The antenna size is 30 cm $\times$ 30 cm. The interelement spacing in DMA is $\lambda/2$, and the numbers of microstrips and metamaterial elements are $N_d = N_e = \lfloor 2D/\lambda \rfloor$, where $\lfloor \cdot \rfloor$ is the integer floor function. We use $\alpha_c = 1.2$ [m^{-1}] and $\beta_c = 827.67$ [m^{-1}] [13], to represent the propagation inside the waveguides. We set $P_{\max}$ to be 1 W, and the RF-to-DC energy conversion efficiency is $\zeta = 0.5$. All wireless channels are generated according to the near-field wireless channel model detailed in [13].

A. Harvested Energy Evaluation

To demonstrate the gains of near-field energy beam focusing over far-field beam steering, Fig. 2 depicts the numerically evaluated normalized received power at each point of the predefined region in the xz-plane, where the normalized

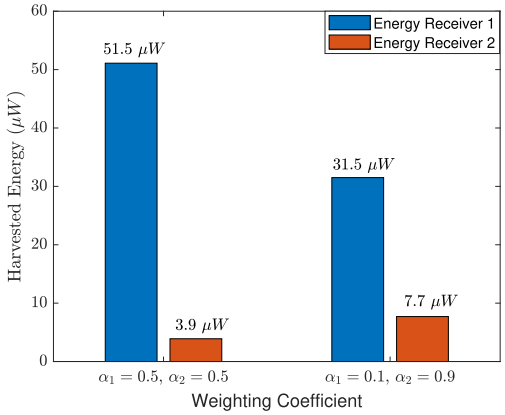

Fig. 3. Comparison of harvested energy of each energy receiver under different combinations of weighting coefficients.

received power is defined as the ratio of the received power of an energy receiver to its corresponding channel gain for removing the influence of path-loss. The energy transmission scheme is designed to maximize the received power of the single energy receiver located at $\mathrm{F}_1(x, y, z) = (0, 0, 1.51$ m). In Fig. 2(a), we set the frequency as 28 GHz, so that the location of the target energy receiver is in the radiating near-field region; whereas in Fig. 2(b), we set the carrier frequency as 1.2 GHz, resulting in the target energy receiver being located in the far-field region. It is observed from Fig. 2(a) that, in the near-field case, the energy beam is focused around the target energy receiver area, and the power harvested by the target energy receiver is up to 13.4 μW. By contrast, for the far-field case as shown in Fig. 2(b), energy can only be transmitted toward a direction with a comparatively wider energy beam. Consequently, far-field signalling results in the target energy receiver harvesting only 6.5 μW, which is only 48% of the power obtained in the near-field. This gain is achieved despite the fact that the system in Fig. 2(b) operates at a lower frequency and hence with a lower isotropic path loss. Besides, by comparing Fig. 2(a) and (b), it is observed that for the radiating near-field WPT system, energy beam focusing is capable of not only enhancing energy transfer efficiency, but also reducing energy pollution.

In Fig. 3, we show the received power of two energy receivers incurred by our proposed Algorithm 1 under different combinations of weighting coefficients. The energy receivers are located at $F_1(x, y, z) = (0, 0, 0.97$ m) and $F_2(x, y, z) = (0, 0, 1.51$ m), lying in a similar angular direction. It is observed from Fig. 3 that for the case of $\alpha_1 = 0.5$, $\alpha_2 = 0.5$, the harvested power of energy receiver 1 is much larger than that of energy receiver 2. This is because energy receiver 1 has a better channel condition and thus energy beams are mainly focused on around its location to maximize the objective for the case of having the same weighting coefficient. When we change the weighting coefficients to $\alpha_1 = 0.1$, $\alpha_2 = 0.9$, the power harvested by energy receiver 2 increases from 3.9 to 7.7 μW, while the power harvested by the energy receiver 1 decreases from 51.5 to 31.5 μW. This is because the energy transmitter is capable of intelligently charging multiple users according to

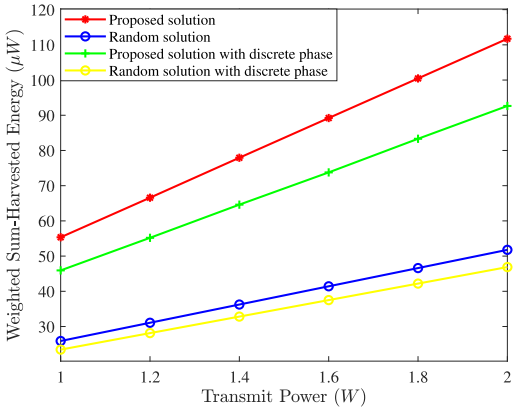

Fig. 4. Weighted sum-harvested energy versus the total transmit power.

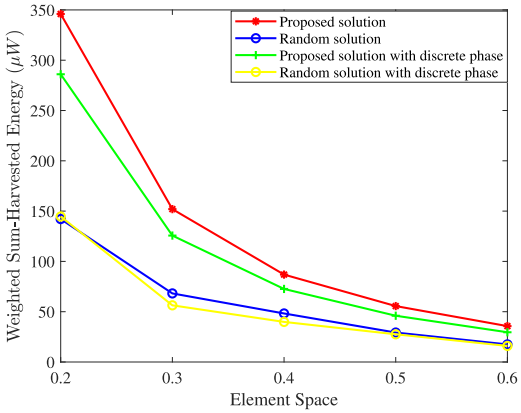

Fig. 5. Weighted sum-harvested energy versus the DMA's antenna element spacing.

their priority/requirements even if multiple energy receivers have similar angular direction, thanks to the distinguishing capability of the near-field energy focusing. We point out that beam steering in the far-field does not possess such distinguishing ability, which is especially important for future 6G IoE applications where devices are expected to be densely deployed in the Fresnel region.

B. Wireless Power Transfer With Discrete DMAs

In the following, we compare the performance of our proposed solution with the random solution, considering both the continuous and discrete phase shifts of DMA elements. For the random solution, which serves as a baseline scheme, we first generate a random DMA configuration and then determine the optimal digital precoding solution based on the given random DMA values. The simulation settings are the same as those used in Fig. 3, with the weighted coefficients set to $\alpha_1 = 0.5$ and $\alpha_2 = 0.5$.

To evaluate the performance, we first compare these solutions in terms of the weighted sum-harvested energy under different values of the transmit power, as shown in Fig. 4. The quantization bit for each DMA element is set to $b = 2$. From Fig. 4, we observe that the proposed solution consistently outperforms the random solution across all scenarios, including both continuous and discrete phase shifts. This demonstrates the significant advantage of jointly optimizing the DMA weights and digital precoding to enhance energy harvesting efficiency. As expected, for all configurations, the weighted sum-harvested energy increases with transmit power, showcasing the scalability of the proposed approach. Additionally, it is observed that the performance of the proposed solution with discrete phase shifts is slightly lower than that of the continuous phase case due to phase quantization.

DMAs leverage metamaterials, enabling subwavelength spacing between elements. Next, as shown in Fig. 5, we study the impact of the DMA antenna element spacing on the weighted sum-harvested energy for different schemes, including both the proposed solution and the random solution, under continuous and discrete phase shift scenarios. The total transmit power is set to 1 W, and the quantization bit for each DMA element is set to $b = 2$. From Fig. 5, we observe that for all solutions, the weighted sum-harvested energy decreases as the element spacing increases. For example, at the smallest element spacing of 0.2λ, the proposed solution with continuous phase shifts achieves the highest energy. This behavior is expected, as larger element spacing reduces the number of antenna elements that can be packed within the given aperture, thereby limiting the energy beam focusing capabilities of the DMA. Moreover, the proposed solution with continuous phase shifts consistently achieves the highest weighted sum-harvested energy across all element spacing values. This demonstrates its ability to efficiently utilize the available aperture and generate highly focused energy beams. The proposed solution with discrete phase shifts follows closely, although it experiences a slight reduction in performance compared to the continuous case due to the phase quantization of DMA elements.

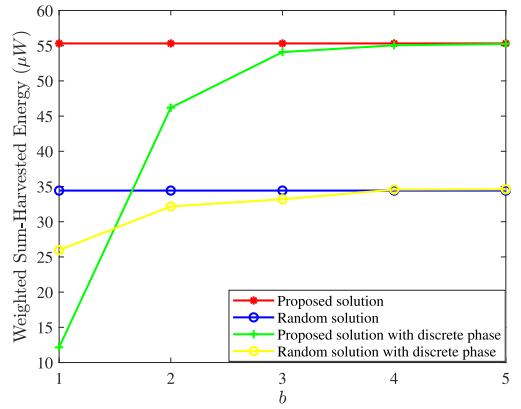

Fig. 6. Weighted sum-harvested energy versus the quantization bit b of the DMA elements.

Fig. 6 illustrates the impact of the quantization bit b on the weighted sum-harvested energy for different solutions. The total transmit power is set to 1 W, and the DMA's element spacing is set to 0.5λ. From Fig. 6, we can see that as the quantization bit b increases, the performance of the proposed solution with discrete phase shifts approaches that of the continuous phase case. For example, at $b = 3$, the weighted sum-harvested energy of the proposed solution with discrete phase shifts is very close to the 55 μW achieved by the

continuous phase solution. This demonstrates that with as few as 3 quantization bits, the proposed solution can achieve near-optimal performance, effectively mitigating the impact of phase quantization.

VI. Conclusion

In this work, we studied the use of DMAs for multiuser wireless power transfer in the radiating near-field region. We presented a model for DMA-based radiating near-field WPT systems, accounting for the unique properties of DMAs as well as spherical wave propagation in the radiating near-field. We then formulated the joint optimization of the DMA weights and digital precoders to maximize the weighted sum-harvested energy and proposed efficient algorithms to solve the resulting nonconvex problems. Moreover, we extended our study to the case of discrete phase shifts in DMA elements, which is essential for practical hardware implementations. Numerical results demonstrated that using DMAs for energy focusing results in improved energy transfer efficiency in the radiating near-field with minimal energy pollution.

Appendix

Proof of Theorem 1

By using the fact that $\mathbf{x}^{\mathrm{T}}\mathbf{Q}\mathbf{y} = (\mathbf{y}^{\mathrm{T}} \otimes \mathbf{x}^{\mathrm{T}})\mathrm{Vec}(\mathbf{Q})$ holds for arbitrary vectors $\mathbf{x}$, $\mathbf{y}$, and matrix $\mathbf{Q}$, the objective function of (13) is rewritten as

$$\zeta \sum_{m=1}^{M} \alpha_m \left|\mathbf{a}_m^H \mathbf{H}\mathbf{Q}\,\mathbf{w}_1\right|^2 = \zeta \sum_{m=1}^{M} \alpha_m \left|\mathbf{z}_m^H \mathbf{q}\right|^2 \tag{22}$$

where $\mathbf{q} = \mathrm{vec}(\mathbf{Q})$ and $\mathbf{z}_m = (\mathbf{w}_1^{\mathrm{T}} \otimes (\mathbf{a}_m^H \mathbf{H}))^H \ \forall m \in \mathcal{M}$, are $N_d^2 \cdot N_e \times 1$ vectors.

As the zero elements of $\mathbf{q}$ have no effect on the value of the right-hand expression in (22), we remove all of them and equivalently rewrite the objective function of (13) as

$$\zeta \sum_{m=1}^{M} \alpha_m \left|\bar{\mathbf{z}}_m^H \bar{\boldsymbol{q}}\right|^2 \tag{23}$$

where $\bar{\boldsymbol{q}}$ is the modified version of $\mathbf{q}$ obtained by removing all the zero elements of $\mathbf{q}$; $\bar{\mathbf{z}}_m$, $m \in \mathcal{M}$, are the modified versions of $\mathbf{z}_m$, which are obtained by removing the elements having the same index as the zero elements of $\mathbf{q}$.

Based on (23), problem (13) is thus simplified as

$$\begin{aligned} \min_{\bar{\boldsymbol{q}}} \ & \bar{\boldsymbol{q}}^H \mathbf{A}(\mathbf{w}_1)\, \bar{\boldsymbol{q}} \\ \text{s.t.} \ & \bar{q}_l \in \mathcal{Q} \ \forall l \in \mathcal{A}_q \end{aligned} \tag{24}$$

where $\mathbf{A}(\mathbf{w}_1) \triangleq -\zeta \sum_{m=1}^{M} \alpha_m \bar{\mathbf{z}}_m \bar{\mathbf{z}}_m^H$, and $\mathcal{A}_q$ denotes the set of all nonzero elements of $\mathbf{q}$.

References

[1] H. Zhang, N. Shlezinger, F. Guidi, D. Dardari, M. F. Imani, and Y. C. Eldar, "Near-field wireless power transfer with dynamic metasurface antennas," in *Proc. IEEE 23rd Int. Workshop Signal Process. Adv. Wireless Commun. (SPAWC)*, 2022, pp. 1–5.

[2] M. Matthaiou, O. Yurduseven, H. Q. Ngo, D. Morales-Jimenez, S. L. Cotton, and V. F. Fusco, "The road to 6G: Ten physical layer challenges for communications engineers," *IEEE Commun. Mag.*, vol. 59, no. 1, pp. 64–69, Jan. 2021.

[3] J. Hu, Q. Wang, and K. Yang, "Energy self-sustainability in full-spectrum 6G," *IEEE Wireless Commun.*, vol. 28, no. 1, pp. 104–111, Feb. 2021.

[4] A. Costanzo and D. Masotti, "Energizing 5G: Near- and far-field wireless energy and data trantransfer as an enabling technology for the 5G IoT," *IEEE Microw. Mag.*, vol. 18, no. 3, pp. 125–136, May 2017.

[5] Y. Zeng, B. Clerckx, and R. Zhang, "Communications and signals design for wireless power transmission," *IEEE Trans. Commun.*, vol. 65, no. 5, pp. 2264–2290, May 2017.

[6] W. Saad, M. Bennis, and M. Chen, "A vision of 6G wireless systems: Applications, trends, technologies, and open research problems," *IEEE Netw.*, vol. 34, no. 3, pp. 134–142, May/Jun. 2020.

[7] S. Hu, F. Rusek, and O. Edfors, "Beyond massive MIMO: The potential of data transmission with large intelligent surfaces," *IEEE Trans. Signal Process.*, vol. 66, no. 10, pp. 2746–2758, May 2018.

[8] F. Guidi and D. Dardari, "Radio positioning with EM processing of the spherical wavefront," *IEEE Trans. Wireless Commun.*, vol. 20, no. 6, pp. 3571–3586, Jun. 2021.

[9] A. Guerra, F. Guidi, D. Dardari, and P. M. Djuric, "Near-field tracking with large antenna arrays: Fundamental limits and practical algorithms," *IEEE Trans. Signal Process.*, vol. 69, pp. 5723–5738, Aug. 2021.

[10] C. You et al., "Next generation advanced transceiver technologies for 6G," 2024, *arXiv:2403.16458*.

[11] P. Nepa and A. Buffi, "Near-field-focused microwave antennas: Near-field shaping and implementation," *IEEE Antennas Propag. Mag.*, vol. 59, no. 3, pp. 42–53, Jun. 2017.

[12] H. Zhang, N. Shlezinger, F. Guidi, D. Dardari, and Y. C. Eldar, "6G wireless communications: From far-field beam steering to near-field beam focusing," *IEEE Commun. Mag.*, vol. 61, no. 4, pp. 72–77, Apr. 2023.

[13] H. Zhang, N. Shlezinger, F. Guidi, D. Dardari, M. F. Imani, and Y. C. Eldar, "Beam focusing for near-field multiuser MIMO communications," *IEEE Trans. Wireless Commun.*, vol. 21, no. 9, pp. 7476–7490, Sep. 2022.

[14] C. Ouyang, Y. Liu, X. Zhang, and L. Hanzo, "Near-field communications: A degree-of-freedom perspective," 2023, *arXiv:2308.00362*.

[15] H. Zhang, N. Shlezinger, F. Guidi, D. Dardari, M. F. Imani, and Y. C. Eldar, "Near-field wireless power transfer for 6G Internet of everything mobile networks: Opportunities and challenges," *IEEE Commun. Mag.*, vol. 60, no. 3, pp. 12–18, Mar. 2022.

[16] K. M. Mayer, L. Cottatellucci, and R. Schober, "Optimal antenna placement for two-antenna near-field wireless power transfer," in *Proc. IEEE Int. Conf. Commun. (ICC)*, 2023, pp. 2135–2140.

[17] E. Demarchou, C. Psomas, and I. Krikidis, "Energy focusing for wireless power transfer in the near-field region," in *Proc. IEEE Glob. Commun. Conf. (GLOBECOM)*, 2022, pp. 4106–4110.

[18] B. J. Deutschmann, T. Wilding, M. Graber, and K. Witrisal, "XL-MIMO channel modeling and prediction for wireless power transfer," in *Proc. IEEE Int. Conf. Commun. Workshops (ICC Workshops)*, 2023, pp. 1355–1361.

[19] Z. Zhang, Y. Liu, Z. Wang, X. Mu, and J. Chen, "Simultaneous wireless information and power transfer in near-field communications," *IEEE Internet Things J.*, vol. 11, no. 16, pp. 27760–27774, Aug. 2024.

[20] N. Song and H. Dai, "Optimal beam-focusing design for 6G near-field SWIPT systems," *IEICE Commun. Exp.*, vol. 13, no. 3, pp. 84–87, Mar. 2024.

[21] Y. Zhang and C. You, "SWIPT in mixed near- and far-field channels: Joint beam scheduling and power allocation," *IEEE J. Sel. Areas Commun.*, vol. 42, no. 6, pp. 1583–1597, Jun. 2024.

[22] Q. Yang, H. Zhang, and B. Wang, "Beamforming design for integrated sensing and wireless power transfer systems," *IEEE Commun. Lett.*, vol. 27, no. 2, pp. 600–604, Feb. 2023.

[23] E. Björnson et al., "Towards 6G MIMO: Massive spatial multiplexing, dense arrays, and interplay between electromagnetics and processing," 2024, *arXiv:2401.02844*.

[24] F. Sohrabi and W. Yu, "Hybrid digital and analog beamforming design for large-scale antenna arrays," *IEEE J. Sel. Topics Signal Process.*, vol. 10, no. 3, pp. 501–513, Apr. 2016.

[25] S. S. Ioushua and Y. C. Eldar, "A family of hybrid analog–digital beamforming methods for massive MIMO systems," *IEEE Trans. Signal Process.*, vol. 67, no. 12, pp. 3243–3257, Jun. 2019.

[26] N. Shlezinger, M. Ma, O. Lavi, N. T. Nguyen, Y. C. Eldar, and M. Juntti, "Artificial intelligence-empowered hybrid multiple-input/multiple-output beamforming: Learning to optimize for high-throughput scalable MIMO," *IEEE Veh. Technol. Mag.*, vol. 19, no. 3, pp. 58–67, Sep. 2024.

[27] A. Jabbar et al., "60 GHz programmable dynamic metasurface antenna (DMA) for next-generation communication, sensing, and imaging applications: From concept to prototype," *IEEE Open J. Antennas Propag.*, vol. 5, pp. 705–726, 2024.

[28] T. Sleasman et al., "Waveguide-fed tunable metamaterial element for dynamic apertures," *IEEE Antennas Wireless Propag. Lett.*, vol. 15, pp. 606–609, 2016.

[29] M. Boyarsky, T. Sleasman, M. F. Imani, J. N. Gollub, and D. R. Smith, "Electronically steered metasurface antenna," *Sci. Rep.*, vol. 11, no. 1, pp. 1–10, 2021.

[30] N. Shlezinger, G. C. Alexandropoulos, M. F. Imani, Y. C. Eldar, and D. R. Smith, "Dynamic metasurface antennas for 6G extreme massive MIMO communications," *IEEE Wireless Commun.*, vol. 28, no. 2, pp. 106–113, Apr. 2021.

[31] H. Wang et al., "Dynamic metasurface antennas for MIMO-OFDM receivers with bit-limited ADCs," *IEEE Trans. Commun.*, vol. 69, no. 4, pp. 2643–2659, Apr. 2021.

[32] R. J. Williams, P. Ramírez-Espinosa, J. Yuan, and E. De Carvalho, "Electromagnetic based communication model for dynamic metasurface antennas," *IEEE Trans. Wireless Commun.*, vol. 21, no. 10, pp. 8616–8630, Oct. 2022.

[33] J. Carlson, M. R. Castellanos, and R. W. Heath, "Hierarchical codebook design with dynamic metasurface antennas for energy-efficient arrays," *IEEE Trans. Wireless Commun.*, vol. 23, no. 10, pp. 14790–14804, Oct. 2024.

[34] Y. Xiu et al., "Robust beamforming design for near-field DMA-NOMA mmWave communications with imperfect position information," *IEEE Trans. Wireless Commun.*, vol. 24, no. 2, pp. 1678–1692, Feb. 2025.

[35] N. Shlezinger, O. Dicker, Y. C. Eldar, I. Yoo, M. F. Imani, and D. R. Smith, "Dynamic metasurface antennas for uplink massive MIMO systems," *IEEE Trans. Commun.*, vol. 67, no. 10, pp. 6829–6843, Oct. 2019.

[36] H. Wang et al., "Dynamic metasurface antennas based downlink massive MIMO systems," in *Proc. IEEE 20th Int. Workshop Signal Process. Adv. Wireless Commun. (SPAWC)*, 2019, pp. 1–5.

[37] D. R. Smith, O. Yurduseven, L. P. Mancera, P. Bowen, and N. B. Kundtz, "Analysis of a waveguide-fed metasurface antenna," *Phys. Rev. Appl.*, vol. 8, no. 5, 2017, Art. no. 54048.

[38] S. W. Ellingson, "Path loss in reconfigurable intelligent surface-enabled channels," 2021, *arXiv:1912.06759*.

[39] J. Xu, L. Liu, and R. Zhang, "Multiuser MISO beamforming for simultaneous wireless information and power transfer," *IEEE Trans. Signal Process.*, vol. 62, no. 18, pp. 4798–4810, Sep. 2014.

[40] X. Yu, D. Xu, and R. Schober, "MISO wireless communication systems via intelligent reflecting surfaces," in *Proc. IEEE/CIC Int. Conf. Commun. China*, 2019, pp. 735–740.

[41] J. Deng, O. Tirkkonen, and C. Studer, "MmWave multiuser MIMO precoding with fixed subarrays and quantized phase shifters," *IEEE Trans. Veh. Technol.*, vol. 68, no. 11, pp. 11132–11145, Nov. 2019.

[42] O. Levy and N. Shlezinger, "Rapid and power-aware learned optimization for modular receive beamforming," 2024, *arXiv:2408.00439*.

[43] B. Di, H. Zhang, L. Song, Y. Li, Z. Han, and H. V. Poor, "Hybrid beamforming for reconfigurable intelligent surface based multi-user communications: Achievable rates with limited discrete phase shifts," *IEEE J. Sel. Areas Commun.*, vol. 38, no. 8, pp. 1809–1822, Aug. 2020.